Computational comparison of fluid-dynamics in carotids before and after endarterectomy

Christian Vergara[1]
Dipartimento di Ingegneria, Università di Bergamo
Viale Marconi 5, 24044, Dalmine (BG), Italy
christian.vergara@unibg.it

Maurizio Domanin
Operative Unit of Vascular Surgery, Fondazione I.R.C.C.S. Ca' Granda Ospedale Maggiore Policlinico di Milano
Department of Clinical Sciences and Community, Università di Milano
Via Sforza 32, 20131, Milan, Italy
maurizio.domanin@unimi.it

Bruno Guerciotti
MOX, Dipartimento di Matematica, Politecnico di Milano
Piazza L. da Vinci 32, 20133, Milan, Italy
bruno.guerciotti@mail.polimi.it

Rocco Michele Lancellotti
MOX, Dipartimento di Matematica, Politecnico di Milano
Piazza L. da Vinci 32, 20133, Milan, Italy
roccomichele.lancellotti@polimi.

Laura Azzimonti
MOXOFF, Spinoff of Politecnico di Milano
Via D'Ovidio Francesco 3, 20131, Milan, Italy
laura.azzimonti@gmail.com

Laura Forzenigo
Radiology Unit, Fondazione I.R.C.C.S. Ca' Granda, Ospedale Maggiore Policlinico di Milano
Via Sforza 32, 20131, Milan, Italy
segrrad@policlinico.mi.it

[1] Tel: +39 0352052314. Fax: +390352052310.

Matteo Pozzoli
AgustaWestland - A Finmeccanica Company
Via Giovanni Agusta 520, 21017, Cascina Costa (VA), Italy
mattepozzoli@gmail.com

Luca Antiga
Orobix s.r.l, Bergamo, Italy
Via L.A. Muratori 3, 24123, Bergamo, Italy
luca.antiga@orobix.com

Piero Biondetti
Radiology Unit, Fondazione I.R.C.C.S. Ca' Granda, Ospedale Maggiore Policlinico di Milano
Via Sforza 32, 20131, Milan, Italy
pibionde@tin.it

ABSTRACT
In this work we provide a computational comparison between the fluid-dynamics before and after carotid endarterectomy (CEA) to assess to influence of this surgical operation on some hemodynamic indices related to the plaque rupture. We perform the numerical simulations in real geometries of the same patients before and after CEA, and with patient-specific boundary data obtained by Echo-color Doppler measurements. The results show a reduction at the systole of the maximum wall shear stress by at least 83%, of the peak velocity by at least 56%, of the vorticity at the internal carotid by at least 57%, and of the pressure gradient across the plaque by at least 83%. Finally, we performed a comparison among measures acquired in internal points and related computed values, highlighting a satisfactory agreement (in any case less than 10%).

INTRODUCTION

Carotids are a preferential site of development of atherosclerotic plaques, leading to vessel stenosis, and, possibly, to a complete obstruction of the vessel, formation of blood clots and breakage with embolization of fragments into the brain tissue [1-4]. For these reasons, carotid endarterectomy (CEA), consisting in the surgical removal of the plaque, is intensively used in the clinical practice. Several studies have highlighted a significant reduction of the stroke risk in patients with severe carotid stenosis who underwent CEA [5-7]. In particular, Doppler measurements and radiological evidences showed that CEA induces a reduction of the peak blood flow velocity and pressure gradients across the plaque [8,9], restoring the physiological haemodynamic conditions. This is an important feature of CEA, since several studies showed that the altered blood fluid-dynamics induced by the stenosis is responsible for the complications related to the plaque formation and rupture. Indeed, it was observed that plaque rupture occurs frequently at the entrance of the stenosis, where the blood forces are elevated [10-13].

For this reason, a comparison of the fluid-dynamics before and after CEA could provide useful information to study the effectiveness of this surgical operation.
Computational methods with patient-specific data have provided an effective tool to investigate quantitatively and non-invasively the fluid-dynamics in carotid arteries since at most two decades. We mention, among the others, [14-19]. In particular, such methods allow to compute the blood velocity and pressure fields, and the forces exerted by the blood.
In this work, we provided, by means of computational tools, a quantitative comparison in three subjects of fluid-dynamics before and after CEA. In particular, we investigated the benefit produced by CEA in terms of reduction of plaque rupture risk. To do this, we performed, both before and after CEA, numerical simulations based on the Finite Element Method (FEM) with patient-specific data (geometries and boundary conditions). This has been possible thanks to the acquisition of radiological images and Echo-Color Doppler signals in the same patient before and after the surgical removal of the plaque. This comparison allowed us to quantify the reduction of peak velocity, vorticity, pressure gradients and viscous forces induced by CEA, providing a concrete evaluation of the effect of this surgical operation on blood fluid-dynamics. The results confirmed that CEA guarantees the restoration of the fluid-dynamic physiological conditions, which prevent plaque breakage.

METHODS

Patients recruitment and carotid endarterectomy

In this study, we considered three carotids of three females (referred to in what follows as patient 1, 2 and 3) with a degree of stenosis greater than 70% and who underwent CEA. This is the surgical treatment for peripheral arterial disease performed most commonly and it can significantly reduce the risk of a stroke in people with severely narrowed carotid arteries [5-7].
All the three patients were followed at Fondazione IRCSS Ca' Granda, Ospedale Maggiore Policlinico, Milan, in particular at the Vascular Surgery Division for the ECD acquisitions and for the surgical treatment, and at the Radiology Division for the radiological acquisitions. Ospedale Maggiore Policlinico follows the recommendations of the Carotid Artery Stenosis Consensus conference [20] for grading carotid stenoses. In particular, stenosis estimate (% diameter reduction, computed comparing the luminal diameter at the site of maximal carotid stenosis and the external diameter at the same site) and peak systolic velocity (PSV) along the internal carotid artery (ICA) are evaluated with the Echo-Color Doppler ultrasound technique as primary parameters. All the CEAs were performed under local anesthesia and the arteriotomies were closed with a Dacron patch.

Acquisition of Echo-Color Doppler signals and boundary conditions

After admission to the hospital, detailed Echo-Color Doppler (ECD) imaging was performed with a 8MHz probe (angle of insonation, 60 degrees; IU22, Philips Ultrasound, Bothwell, U.S.A.) by an experienced user (M.D). In all the cases, the measures have been acquired at the center of the vessel and with a beam-to-flow angle as small as possible, so to obtain measures of the velocity along the longitudinal direction. The measurement of the velocity were made in the ICA (2 cm downstream from the site of maximum stenosis), and in the common carotid artery (CCA; 2 cm retrograde from the bifurcation). For CCA we acquired the signal at several time steps for some heartbeats, whereas for the ICA the signal was acquired only at systole. Carotid diameters were measured on a captured screen image with B mode ultrasound scanning and placement of cursors to give a read out in millimeters. This allowed to compute the percentage of stenosis which, together with peak systolic velocity and ultrasound scanning, defined the severity of stenosis with respect to the luminal diameter. In Table 1 we summarize the data related to the three patients. The same ECD acquisitions were performed also after CEA, so that in fact we have at disposal, for each patient, velocity signals both before and after CEA.

To generate from ECD signals suitable patient-specific velocity profiles in view of the numerical simulations, we proceeded as follows. The ECD signal represents the histograms of the velocities measured at the center of a given section, where, for any fixed time, the gray-scaled intensity of pixels is proportional to the number of blood-cells moving at a certain velocity (see Figure 1, up). We first estimated for each time instants the maximum velocity on the section at hand, using the 95-th quantile of the velocity histogram as a robust estimator. Then, we used a Fourier smoothing of the time signal along three heartbeats, obtained by the projection of the time signal on a Fourier basis (see Figure 1, bottom). Further details are reported in [21,22].

Once the velocity at the center of the CCA cross section has been provided by the elaboration of the ECD signals, we made the assumption that at each time step this velocity corresponds to the (spatial) maximum one over the section, in the following named $V_{MAX\text{-}CCA}(t)$. Then, we estimated the flow rate $Q_{CCA}(t)$ at each time step by using the formula proposed in [23] and validated in [24,25]:

$$Q_{CCA}(t) = A_{CCA} * K(t) * V_{MAX\text{-}CCA}(t), \qquad (1)$$

where A_{CCA} is the area of the CCA section and K(t) is a suitable parameter which depends on the Womersley number, and thus on the pulsatility of the signal, and accounts for the shape of the spatial profile. For example, K=0.5 is related to a parabolic profile on a circular section.

Now, to prescribe this flow rate, in absence of any radiological information about the spatial velocity distribution, we assumed a parabolic profile, as suggested in [26]. To set the corresponding maximum velocity $V_{PAR\text{-}CCA}(t)$ under this assumption, we considered the maximum circle C_{CCA} inscribed in the CCA section, and we set

$$V_{PAR\text{-}CCA}(t) = 2 * Q_{CCA}(t) / A_{C\text{-}CCA} = 2 * A_{CCA} / A_{C\text{-}CCA} * K(t) * V_{MAX\text{-}CCA}(t),$$

where $A_{C\text{-}CCA}$ is the area of C_{CCA}. The previous equation gave us a relation to obtain the velocity values to be prescribed as inlet boundary condition ($V_{PAR\text{-}CCA}(t)$) starting from the velocities reconstructed from ECD ($V_{MAX\text{-}CCA}(t)$). Then, the desired inlet boundary condition has been obtained at each time step by considering the parabola defined on C_{CCA} with maximum value equal to $V_{PAR}(t)$ at the center of C_{CCA} and zero values at the boundary of C_{CCA}. For the points of the CCA section not belonging to C_{CCA}, we assumed a null velocity. All this procedure has been performed both for the pre-operative data and for the post-operative data.
As for the outlet condition at the ICA section, we had at disposal only the systolic value, thus we proceeded as follows. We first estimated the flow rate $Q_{ICA}(t_{sys})$ using a formula analogous to (1) at the systolic time instant t_{sys}. Then, we computed the systolic flow division $\alpha = Q_{ICA}(t_{sys})/ Q_{CCA}(t_{sys})$ and we generated the flow rate $Q_{ICA}(t)$ defined by $Q_{ICA}(t)= \alpha^* Q_{CCA}(t)$, assuming that the flow division does not depend on the instant of the cardiac cycle. Then, we assumed again a parabolic velocity profile in the circle C_{ICA} inscribed in the ICA section, thus estimating at each time step the maximum velocity as $V_{PAR\text{-}ICA}(t) = 2^*Q_{ICA}(t)/A_{C\text{-}ICA} = 2\alpha^*Q_{CCA}(t)/A_{C\text{-}ICA,}$ where $A_{C\text{-}ICA}$ is the area of C_{ICA}. Again, for the points of the ICA section not belonging to C_{ICA}, we assumed a null velocity.
As for the boundary condition at ECA we prescribed zero tractions (homogeneous Neumann condition), since we are assuming rigid walls (see the next subsection).

Acquisition of radiological images and mesh generation
The radiological acquisitions were performed with a Siemens 1.5T Avanto MR scanner. For each patient we acquired a volume ranging from the level of the aortic arch to the level of the circle of Willis to include the carotid arteries. We used the following sequencies and planes: Turbo Spin Echo T 1 weighted axial images, True Fisp single shot axial and coronal images, Turboflash 2D rectrospectively elettrocardiographic (ECG) gated axial images, phase contrast axial images at the stenosis level and immediately cranial and caudal from the stenosis level. The ECG gated axial images were reconstruted every ten per cent of the R-R interval from aortic arch to the circle of Willis. Finally we acquired Gradient Echo T1 weighted 3D Fat Sat images before and during injection of paramagnetic contrast medium (gadolinium) in coronal plane to study the carotids artery from aortic arch to the circle of Willis. All this procedure has been performed for all the three patients both before and after CEA.
A surface model of the interface between the blood and the arterial wall of the six carotids have then been obtained from the radiological images, using a level-set segmentation technique provided by the Vascular Modeling Toolkit (vmtk, http://www.vmtk.org). The surface models were successively turned into volumetric meshes of linear tetrahedra in view of computational fluid-dynamics (CFD) simulations.

Numerical simulations
Unsteady numerical simulations have been performed by using the finite element library LifeV (http://www.lifev.org). Blood was considered as Newtonian, homogeneous, and incompressible, and the Navier–Stokes equations for incompressible fluids were

considered [27]. Blood viscosity was 0.035 Poise, fluid density 1.0 g/cm^3 and the time step 0.01s. Moreover, we used P1bubble/P1 finite elements for the space discretization, and the backward Euler method with a semi-implicit treatment of the convective term for the temporal discretization. For results independency, we tested that the results remained the same, up to a suitable tolerance, when reducing the time step or refining the mesh. The vessel wall was considered rigid, since we do not expect that the dynamics of the wall substantially affects the results of the comparisons we have in mind (see Discussion above). We also highlighted that no turbulence models were assumed. This is of course a limitation for the stenotic cases, which will be discussed in the Discussion.

RESULTS

As for the mesh size, we have 97396 and 128831 tetrahedra for case 1 before and after CEA, respectively; 165334 and 100076 tetrahedra for case 2 before and after CEA, respectively; 323247 and 289479 tetrahedra for case 3 before and after CEA, respectively. These mesh sizes were set after a mesh refinement study, with the aim of obtaining a mesh-independent numerical solution.

In Figure 2 we plotted the behavior in time of the velocities $V_{PAR\text{-}CCA}(t)$ and $V_{PAR\text{-}ICA}(t)$ generated starting from the ECD signals and prescribed as maximum velocity in the parabolic profile for each patients, both before and after CEA. The systolic flow division α between CCA and ICA was 0.88 for patient 1, 0.72 for patient 2, and 0.81 for patient 3.

In Figure 3 we depicted the streamlines of the velocity field at the systole for all the three patients, both before and after CEA. We observe that the velocity obtained before CEA is higher than the one obtained after CEA, due to the presence of a severe stenoses. This has been also confirmed by the values of the peak systolic velocity (PSV), intended as the maximum value reached inside the domain at the systole, reported in Table 2. From Figure 3 we also observe that the non-physiological morphology of the pre-CEA carotids, induced by the presence of the atherosclerotic plaque, causes the development of helical patterns, particularly visible at the ICA (zoomed in the figures). As it is evident in this figure, these helical patterns are not visible in the post-CEA ICAs. To confirm this, in Figure 4 we reported the systolic vorticity field in the three patients, whereas in Table 3 the maximum systolic vorticity in the ICA. These results confirmed the presence of vortices at the ICA during the systole (high vorticity) before CEA, which are quite absent (low vorticity) after CEA.

In Figure 5 we showed the WSS at the systole, whereas in Table 4 we reported the maximum systolic WSS in the region of the plaque, which corresponds to the bifurcation. Again, we observe significantly higher values featured by the configuration before CEA with respect to the one after CEA, in particular in the regions where the plaque was present.

In Table 5 we reported the values of the systolic pressure gradient across the plaque. Since the exact localization of the atherosclerotic plaque is rather complicated from the medical images, the systolic pressure drop between the CCA and the ICA was

considered. We observe that the values of the pressure drop are significantly lower after CEA, due to the widening of the lumen that decreases the resistance opposed to blood flow.

To assess the accuracy of our results, we compared the systolic velocity field computed by our simulations with available ECD measures not used in the numerical experiments. In particular, we had at disposal from ECD exams the measurements of the maximum velocity at some internal cross sections, namely at the level of the bifurcation for Patient 1 and 3 before CEA, at the begin of the ICA for Patients 1 and 3 after CEA, at a distance of 0.5cm from the begin of the ICA for Patient 2 before CEA, and at a distance of 1.0cm from the begin of the ICA for Patient 2 after CEA. To obtain the peak systolic velocity from these signals, we proceeded as done for the boundary conditions, by using the 95-th quantile of the velocity histogram. Again, the measures have been acquired at the center of the vessel and along the longitudinal direction. In view of the comparison, we selected a cylinder of 2mm of height with center located in the measurement point, and we took the maximum computed velocity within this cylinder. In Table 6 we reported the results of this comparison for each of the six considered cases. These results highlighted a very good accordance between measures and computation.

DISCUSSION

State of the art and choice of the computational model

In this work we provided a computational comparison of the fluid-dynamics in carotids before and after the plaque removal, for three subject who underwent CEA. Computational studies in human carotids have been performed since 25 years, see the pioneering work [14]. Many other works have focused on this issue using patient-specific data. Among the ones who used the rigid wall assumption, we mention [28, 15, 29, 19, 26, 30]. More recently, other studies have focused on the mechanical stresses, thus relying on the solution of a fluid-structure interaction (FSI) problem, see, e.g., [16, 31, 18, 32-34]. In this work, we considered the rigid walls assumptions, since we were interested in haemodynamic quantities. In [17], a comparison between simulations in carotids obtained both in rigid and in deformable domains highlighted that some differences occur when computing haemodynamic quantities. For example, the computation of the oscillatory shear index (OSI, not used in this work) seems to be strongly affected by the inclusion of wall compliance. Instead, WSS seems to be little sensitive to the wall assumptions (see also [35]). In any case, since in this work we focused on a comparison between two scenarios (namely the configurations before and after CEA), rather than on the precise quantification of some quantity, we believe that the results should not be influenced so much by the wall assumption, so that, for the sake of simplicity, rigid simulations have been performed. We also notice that a FSI study for the pre-operative cases should need the knowledge of the location of the plaque and of the quantification of its physical parameters, both hardly measurable with standard techniques.

In this work we also prescribed patient-specific boundary conditions obtained by Echo-Color Doppler acquisitions. The prescription of patient-specific data at the artificial sections, namely those generated by the truncation of the computational domain, is a fundamental issue in view of obtaining accurate numerical results [15]. For example, in [29] the authors showed that some fluid-dynamic quantity (such as the negative axial velocity region, NAVR) could be computed erroneously if no patient-specific data are used, whereas in [19] the authors highlighted that the Murray's law for the flow division, holding for a normal carotid, is not anymore valid for stenotic carotids, thus implying the need of using patient-specific data. As for our choice of prescribing a parabolic velocity profile, we mention [26], where the authors recommend for accuracy purposes, in absence of information about the spatial profile, this choice over the blunt or Womersley ones.

We also considered no turbulence models in our computations. This choice is perfectly justified for the post-operation cases, where the flow is laminar. However, for the pre-operation cases with a degree of stenosis greater than 70%, the use of a turbulent model should be considered [36], although recent computational studies in stenotic carotids did not consider turbulent models (e.g., [37]). Experimental studies highlighted that the endothelium is considerably more sensitive to relatively low shear stresses in turbulent flow than to higher shear stresses applied in laminar flow [38]. This suggested that the risk of rupture should increase when turbulent flows were considered, thus resulting in a possible marked improvement of the benefit of CEA with respect to what predicted by our results. For this reason, in this preliminary study we considered no turbulence models.

Haemodynamic quantities to assess the risk of plaque rupture

While atherosclerosis is a long and gradual process, plaque rupture is rapid and, in most cases, unpredictable. To assess the state of development of the plaque, the degree of stenosis is probably the easiest indicator to be evaluated by clinicians. Unfortunately, percent stenosis cannot be considered an appropriate risk indicator of the plaque rupture [39]. Structural quantities related to plaque rupture, such as wall stresses, could be evaluated by means of FSI simulations [40,41]. Here we focused on haemodynamic indices, in particular the Wall Shear Stresses (WSS), the spatial pressure gradient and the systolic peak velocity.

It is known that high values of the WSS could induce plaque rupture [42,12]. In particular, high WSS acting on the endothelium has a regressive effect on the underlying intimal tissue, inducing an anti-proliferative action which may lead to cap thinning and, thus, enhancing plaque vulnerability. Another quantity which has been correlated to plaque rupture is the pressure gradient across the plaque [43,13]. The pressure drop across the plaque induced by the stenosis, in particular at the systole, might deform a vulnerable plaque and induce substantial axial strain, resulting possibly in plaque rupture. In this sense, while high WSS are hypothesized to modulate local biological processes that destabilize the plaque, making it more prone to rupture, pressure drop might act as the main mechanical trigger for the rupture of weakened upstream regions. Finally, we considered the maximum (peak) velocity at the systole, which is easily

measurable with the ECD technique and often used by clinicians. In particular, velocities higher than 200 cm/s are considered dangerous in view of the plaque rupture.

Computational comparison before and after CEA

In [44], the authors investigated changes in physical quantities in carotid arteries before and after CEA, using image-based technologies. In particular, they considered indicators that are correlated to plaque formation, whereas no attention was given to the risk of plaque rupture. Here we reported, at the best of our knowledge, the first attempt to perform a patient-specific comparison, before and after CEA, of fluid-dynamic quantities related to the risk of plaque rupture by means of computational tools.

From the results obtained in the configurations before CEA, we observed high non-physiological values of the systolic velocity, maximum WSS and pressure drop across the plaque, induced by the severe stenoses characterizing the three patients. The PSV showed values which are more than two times greater (3 times for patients 1 and 3) than the physiological ones, whereas the maximum WSS values are almost 10 times greater than the physiological ones. Moreover, the streamlines and the vorticity highlighted an abnormal fluid-dynamics at the systole, in particular at the ICA, where helicoidal structures appeared, generating high WSS also in this region. This is clearly a non-physiological condition characterized by vortices at high energy, which could have a negative effect on the vessel structure and on the cerebral circulation.

As for the effect of CEA, from our results it was evident the effect of the surgical removal of the plaque and of the patch seam, which contribute to a substantial widening of the vessel lumen, thus causing blood velocity (and, hence, velocity gradients) and pressure drop to decrease significantly. In particular, as for the systolic peak velocity, we observed a reduction of 64.9%, 69.7%, and 55.9% in the three patients due to CEA, restoring a physiological PSV of about 100 cm/s. Moreover, CEA was able to eliminate the systolic helicoidal structures arising in the ICA, producing a reduction of 57.7%, 81.6%, and 59.4% in the maximum systolic vorticity, and thus restoring the normal systolic conditions characterized by a fluid-dynamics in the ICA, which is laminar and aligned with the longitudinal axis. Even though some helicity may be present at the level of the bifurcation in the post-CEA cases, due to the enlargement of the vessel lumen after plaque removal and patch reconstruction, blood flow seems to recover physiological conditions after the bifurcation and in the ICA. Thus, beside causing a significant decrease in maximum velocity magnitude, CEA also contributes to the restoration of physiological conditions at the ICA, preventing the development of abnormal flow patterns that may interfere negatively with the cerebral circulation and possibly causing brain damage.

As for the maximum WSS at the level of the bifurcation, we observed a reduction of 86.8%, 83.2%, and 84.3% in the three patients induced by CEA, restoring the physiological conditions characterized by a value of the maximum WSS of about 3-5 Pa. Obviously, a strong reduction of WSS magnitude at the level of the bifurcation may predispose to the risk of atherosclerotic plaque re-formation [45], but this circumstance is surely much less dangerous than the risk of plaque breakage, which is promoted by the high values of WSS.

Finally, we observed also a reduction after CEA of the systolic pressure drop between CCA and ICA of 89.0%, 88.3%, and 83.5% in the three patients. Since high pressure drops seem to be the main cause of plaque breakage, these results confirmed the benefit of CEA in view of preventing the rupture.

Validation of the numerical results

Finally, we performed a comparison between available ECD measures at internal cross sections (not used in the numerical experiments) and the corresponding computed values. The results of Table 6 showed the following discrepancies: 4.8% and 8.7% for Patient 1, 8.0% and 10.5% for Patient 2, 4.8% and 4.6% for Patient 3. These results, although far to establish a complete validation, are very interesting since highlighted the accuracy, at least where measurements were available, of our numerical simulations. This made our results and the related conclusions about CEA highly reliable.

Limitations

As emerged from the Discussion, three major limitations characterized the present work. First of all, the use of rigid walls, although justified as explained in the Discussion, should be replaced by the hypothesis of compliant walls, thus relying to the solution of an FSI problem which should allow to compute more accurate results. Secondly, the hypothesis of parabolic profile, although justified as discussed in [26], is of course an approximation and should be replaced by using spatial in-vivo data, obtained for example from PC-MRI. Finally, the use of no turbulence models seems to be not adequate for the stenotic cases. For all these reason, we are studying, for future works, which are the main effects of the inclusion of FSI models, spatial in-vivo velocity profiles, and large eddy simulations (LES) models in the study of CEA.

BIBLIOGRAPHY

[1] Timsit, S.G., Sacco, R.L., Mohr, J.P., Foulkes, M.A., Tatemichi, T.K., Wolf, P.A., Price, T.R., and Hier, D.B., 1992, "Early clinical differentiation of cerebral infarction from severe atherosclerotic stenosis and cardioembolism", Stroke, **23**(4), pp. 486-91. DOI: 10.1161/01.STR.23.4.486

[2] Wootton, D.M., and Ku, D.N., 1999, "Fluid mechanics of vascular systems, diseases, and thrombosis", Ann. Rev. Biomed. Eng., **1**, pp. 299-329. DOI: 10.1146/annurev.bioeng.1.1.299

[3] Rauch, U., Osende, J.I., Fuster, V., Badimon, J.J., Fayad, Z., and Chesebro, J.H., 2001, "Thrombus Formation on Atherosclerotic Plaques: Pathogenesis and Clinical Consequences", Annals of Internal Medicine, **134,** pp. 224-238. DOI: 10.7326/0003-4819-134-3-200102060-00014

[4] Falk, E., 2006, "Pathogenesis of Atherosclerosis", Journal of American College of Cardiology, **47**(8), pp. C7-12. DOI: 10.1016/j.jacc.2005.09.068

[5] Executive Committee for the Asymptomatic Carotid Atherosclerosis Study, 1995, "Endarterectomy for asymptomatic carotid artery stenosis", JAMA, **273**(18), pp. 1421-1428. DOI: 10.1001/jama.1995.03520420037035

[6] Barnett, H.J., Taylor, D.W., Eliasziw, M., Fox, A.J., Ferguson, G.G., Haynes, R.B., Rankin, R.N., Clagett, G.P., Hachinski, V.C., Sackett, D.L., Thorpe, K.E., Meldrum, H.E., and Spence, J.D, 1998, "Benefit of carotid endarterectomy in patients with symptomatic moderate or severe stenosis", North American Symptomatic Carotid Endarterectomy Trial Collaborators", N. Engl. J. Med., **339**(20), pp. 1415-1425. DOI: 10.1056/NEJM199811123392002

[7] ECST, 1998, "Randomised trial of endarterectomy for recently symptomatic carotid stenosis: final results of the MRC European Carotid Surgery Trial (ECST)", Lancet, **351**, pp. 1379-1387. DOI: 10.1016/S0140-6736(97)09292-1

[8] Steinke, W., Hennerici, M., Kloetzsch, C., and Sandmann, W., 1991, "Doppler colour flow imaging after carotid endarterectomy" Eur. J. Vasc. Surg., **5**(5), pp. 527-534. DOI: 10.1016/S0950-821X(05)80340-8

[9] Harloff, A**.**, Zech, T**.**, Wegent, F**.**, Strecker, C**.**, Weiller, C**.**, and Markl, M**.**, 2013, "Comparison of blood flow velocity quantification by 4D flow MR imaging with ultrasound at the carotid bifurcation", Am. J. Neuroradiol**., 34**(7), pp. 1407-1413. DOI: 10.3174/ajnr.A3419

[10] Stroud, J.S., Berger, S.A., and Saloner, D., 2000, "Influence of stenosis morphology on flow through severely stenotic vessels: implications for plaque rupture", J. Biomech., **33**(4), pp. 443-55. DOI: 10.1016/S0021-9290(99)00207-9

[11] Lovett, J.K., and Rothwell, P.M., 2003, "Site of carotid plaque ulceration in relation to direction of blood flow: an angiographic and pathological study", Cerebrovasc. Dis., **16**(4), pp. 369-75. DOI: 10.1159/000072559

[12] Groen, H.C., Gijsen, F.J., van der Lugt, A., Ferguson, M.S., Hatsukami, T.S., van der Steen, A.F., Yuan, C., and Wentzel, J.J., 2007, "Plaque rupture in the carotid artery is localized at the high shear stress region: a case report", Stroke, **38**(8), pp. 2379-2381. DOI: 10.1161/STROKEAHA.107.484766

[13] Dolan, J.M., Kolega, J., and Meng, H., 2013, "High wall shear stress and spatial gradients in vascular pathology: a review", Ann. Biomed. Eng., **41**(7), pp. 1411-1427. DOI: 10.1007/s10439-012-0695-0

[14] Perktold, K., and Resch, M., 1990, "Numerical flow studies in human carotid artery bifurcations: basic discussion of the geometric factor in atherogenesis", J. Biomed. Eng., **12**(2), pp. 111-123. DOI: 10.1016/0141-5425(90)90131-6

[15] Milner, J.S., Moore, J.A., Rutt, B.K., and Steinman, D.A., 1998, "Hemodynamics of human carotid artery bifurcations: computational studies with models reconstructed from magnetic resonance imaging of normal subjects", J. Vasc. Surg., **28**(1), pp. 143-156.

[16] Tang, D., Yang, C., Zheng, J., Woodard, P.K., Sicard, G.A., Saffitz, J.E., and Yuan, C., 2004, "3D MRI-based multicomponent FSI models for atherosclerotic plaques", Ann. Biomed. Eng., **32**(7), pp. 947-960. DOI: 10.1023/B:ABME.0000032457.10191.e0

[17] Younis, H.F., Kaazempur-Mofrad, M.R., Chan, R.C., Isasi, A.G., Hinton, D.P., Chau, A.H., Kim, L.A., and Kamm, R.D., 2004, "Hemodynamics and wall mechanics in human carotid bifurcation and its consequences for atherogenesis: investigation of inter-individual variation", Biomech. Model. Mechanobiol., **3**(1), pp. 17-32. DOI: 10.1007/s10237-004-0046-7

[18] Gao, H., Long, Q., Graves, M., Gillard, J.H., and Li, Z.Y., 2009, "Carotid arterial plaque stress analysis using fluid-structure interactive simulation based on in-vivo magnetic resonance images of four patients", J. Biomech., **42**(10), pp. 1416-1423. DOI: 10.1016/j.jbiomech.2009.04.010

[19] Groen, H.C., Simons, L., van den Bouwhuijsen, Q.J., Bosboom, E.M., Gijsen, F.J., van der Giessen, A.G., van de Vosse, F.N., Hofman, A., van der Steen, A.F., Wittemanm J.C., van der Lugtm A., and Wentzel, J.J., 2010, "MRI-based quantification of outflow boundary conditions for computational fluid dynamics of stenosed human carotid arteries", J. Biomech., **43**(12), pp. 2332-2338. DOI: 10.1016/j.jbiomech.2010.04.039

[20] Grant, E.G., Benson, C.B., Moneta, G.L., Alexandrov, A.V., Baker, J.D., Bluth, E.I., Carroll, B.A., Eliasziw, M., Gocke, J., Hertzberg, B.S., Katanick, S., Needleman, L., Pellerito, J., Polak, J.F., Rholl, K.S., Wooster, D.L., and Zierler, E., 2003, "Carotid Artery Stenosis: Gray-Scale and Doppler US Diagnosis - Society of Radiologists in Ultrasound Consensus Conference", Radiology, **229**, pp. 340-346. DOI: 10.1148/radiol.2292030516

[21] Buratti, P., 2011, "Analysis of Doppler blood flow velocity in carotid arteries for the detection of atherosclerotic plaques", MSc thesis, http://mox.polimi.it/it/progetti/pubblicazioni/viewtesi.php?id=516&en=en

[22] Azzimonti, L., 2013, "Blood flow velocity field estimation via spatial regression with PDE penalization", PhD thesis, Politecnico di Milano, Italy

[23] Ponzini, R., Vergara, C., Redaelli, A., and Veneziani, A., 2006, "Reliable CFD-based estimation of flow rate in haemodynamics measures", Ultrasound in Med. and Biol., **32** (10), pp. 1545-1555. DOI: 10.1016/j.ultrasmedbio.2006.05.022

[24] Vergara, C., Ponzini, R., Veneziani, A., Redaelli, A., Neglia, D., and Parodi, O., 2010, "Womersley number-based estimation of flow rate with Doppler Ultrasound: Sensitivity analysis and first clinical application", Computer Methods and Programs in Biomedicine, **98**(2), pp. 151-160. DOI: 10.1016/j.cmpb.2009.09.013

[25] Ponzini, R., Vergara, C., Rizzo, G., Veneziani, A., Roghi, A., Vanzulli, A., Parodi, O., and Redaelli, A., 2010, "Womersley number-based estimates of blood flow rate in Doppler analysis: In vivo validation by means of Phase Contrast Magnetic Resonance Imaging", IEEE Transaction on Biomedical Engineering, **57** (7), pp. 1807-1815. DOI: 10.1109/TBME.2010.2046484

[26] Campbell, I.C., Ries, J., Dhawan, S.S., Quyyumi, A.A., Taylor, W.R., and Oshinski, J.N., 2012, "Effect of inlet velocity profiles on patient-specific computational fluid dynamics simulations of the carotid bifurcation", J. Biomech. Eng., **134**(5), pp. 051001. DOI: 10.1115/1.4006681

[27] Formaggia, L., Quarteroni, A., and Veneziani, A. (eds), 2009, *Cardiovascular mathematics: modeling and simulation of the circulatory system, modeling, simulation and applications*, Springer, Milan, Italy. ISBN: 978-88-470-1152-6

[28] Perktold, K., Thurner, E., and Kenner, T., 1994, "Flow and stress characteristics in rigid walled and compliant carotid artery bifurcation models", Med. Biol. Eng. Comput., **32**(1), pp. 19-26. DOI: 10.1007/BF02512474

[29] Wake, A.K., Oshinski, J.N., Tannenbaum, A.R., and Giddens, D.P., 2009, "Choice of in vivo versus idealized velocity boundary conditions influences physiologically relevant flow patterns in a subject-specific simulation of flow in the human carotid bifurcation", J. Biomech. Eng., **131**(2), pp. 021013. DOI: 10.1115/1.3005157

[30] Dong, J., Wong, K.K.L., and Tu, J., 2013, "Hemodynamics analysis of patient-specific carotid bifurcation: A CFD model of downstream peripheral vascular impedance", Int. J. Num. Meth. Biomed. Eng., **29**(4), pp. 476–491. DOI: 10.1002/cnm.2529

[31] Kock, S.A., Nygaard, J.V., Eldrup, N., Fründ, E.T., Klaerke, A., Paaske, W.P., Falk, E., and Yong Kim, W., 2008, "Mechanical stresses in carotid plaques using MRI-based fluid-structure interaction models", J. Biomech., **41**(8), pp. 1651-1658. DOI: 10.1016/j.jbiomech.2008.03.019

[32] Kural, M.H., Cai, M., Tang, D., Gwyther, T., Zheng, J., and Billiar, K.L., 2012, "Planar biaxial characterization of diseased human coronary and carotid arteries for

computational modeling", J. Biomech., **45**(5), pp. 790-798. DOI: 10.1016/j.jbiomech.2011.11.019

[33] Lee, S.H., Kang**,** S., Hur**,** N., and Jeong**,** S.K., 2012, "A fluid-structure interaction analysis on hemodynamics in carotid artery based on patient-specific clinical data", J. Mech. Sci. Tech., **26**(12), pp. 3821-3831. DOI: 10.1007/s12206-012-1008-0

[34] Kamenskiy, A.V., Mactaggart, J.N., Pipinos, I.I., Gupta, P.K., and Dzenis, Y.A., 2013, "Hemodynamically motivated choice of patch angioplasty for the performance of carotid endarterectomy", Ann. Biomed. Eng., **41**(2), pp. 263-278. DOI: 10.1007/s10439-012-0640-2

[35] Steinman, D.A., and Ethier, C.R., 1994, "The effect of wall distensibility on flow in a two-dimensional end-to-side anastomosis", J. Biomech. Eng., **116**(3), pp. 294-301. DOI: 10.1115/1.2895733

[36] Ku, D.N., 1997, "Blood flow in arteries", Annu. Re. Fluid Mech., **29**, pp. 399-434. DOI: 10.1146/annurev.fluid.29.1.399

[37] Bark, D.L. Jr, and Ku, D.N., 2010, "Wall shear over high degree stenoses pertinent to atherothrombosis", J. Biomech., **43**(15), pp. 2970-2977. DOI: 10.1016/j.jbiomech.2010.07.011

[38] Davies, P.F**.**, Remuzzi, A**.**, Gordon, E.J**.**, Dewey, C.F. Jr, and Gimbrone, M.A. Jr., 1986, **"**Turbulent fluid shear stress induces vascular endothelial cell turnover in vitro", Proc. Natl. Acad. Sci. U S A, **83**(7), pp. 2114-2117.

[39] Makris, G.C., Nicolaides, A.N., Xu, X.Y., and Geroulakos, G., 2010, "Introduction to the biomechanics of carotid plaque and rupture: review of the clinical evidence", The British Journal of Radiology, **83**, pp. 729-735. DOI: 10.1259/bjr/49957752

[40] Tang, D., Teng, Z., Canton, G., Yang, C., Ferguson, M., Huang, X., Zheng, J., Woodard, P.K., and Yuan, C., 2009, "Sites of rupture in human atherosclerotic carotid plaques are associated with high structural stresses: an in vivo MRI-based 3D fluid-structure interaction study", Stroke, **40**(10), pp. 3258-3263. DOI: 10.1161/STROKEAHA.109.558676

[41] Gao, H., Long, Q., Das, S.K., Sadat, U., Graves, M., Gillard, J.H., and Li, Z.Y., 2011, "Stress analysis of carotid atheroma in transient ischemic attack patients: evidence for extreme stress-induced plaque rupture", Ann. Biomed. Eng., **39**(8), pp. 2203-2212. DOI: 10.1007/s10439-011-0314-5

[42] Slager, C.J., Wentzel, J.J., Gijsen, F.J., Thury, A., van der Wal, A.C., Schaar, J.A., and Serruys, P.W., 2005, "The role of shear stress in the destabilization of vulnerable plaques

and related therapeutic implications", Nat. Clin. Pract. Cardiovasc. Med., **2**(9), pp. 456-464. DOI: 10.1038/ncpcardio0298

[43] Li, Z.Y., and Gillard, J.H., 2008, "Plaque rupture: plaque stress, shear stress, and pressure drop", Journal of the American College of Cardiology, **52**(13), pp. 1106-1107. DOI: 10.1016/j.jacc.2008.08.004

[44] Harloff, A., Berg, S., Barker, A.J., Schöllhorn, J., Schumacher, M., Weiller, C., and Markl, M., 2013, "Wall shear stress distribution at the carotid bifurcation: influence of eversion carotid endarterectomy", Eur. Radiol., **23**(12), pp. 3361-3369. DOI: 10.1007/s00330-013-2953-4

[45] Ku, D.N., Giddens, D.P., Zarins, C.K., and Glagov, S., 1985, "Pulsatile flow and atherosclerosis in the human carotid bifurcation. Positive correlation between plaque location and low oscillating shear stress", Arteriosclerosis, **5**(3), pp. 293-302. DOI: 10.1161/01.ATV.5.3.293

Figure Captions List

Fig. 1 Example of Echo-Color Doppler signal (up) and of the maximum velocity extraction (bottom)

Fig. 2 Maximum velocities $V_{PAR\text{-}CCA}(t)$ (up) and $V_{PAR\text{-}ICA}(t)$ (bottom) for patient 1 (left), patient 2 (middle), and patient 3 (right).

Fig. 3 Streamlines of the velocity field at the systole. From the left to the right: patient 1, patient 2 and patient 3. Up: before CEA; bottom: after CEA.

Fig. 4 Vorticity at the systole. From the left to the right: patient 1, patient 2 and patient 3. For each patient, on the left the case before CEA, o the right the case after CEA.

Fig. 5 Wall shear stress at the systole. From the left to the right: patient 1, patient 2 and patient 3. For each patient, on the left the case before CEA, o the right the case after CEA.

Table Caption List

Table 1 Data related to the three patients.

Table 2 Values of the peak systolic velocity for the three patients before and after CEA

Table 3 Maximum systolic vorticity at the ICA for the three patients before and after CEA

Table 4 Maximum systolic WSS at the bifurcation for the three patients before and after CEA

Table 5 Systolic pressure drop between ICA end CCA for the three patients before and after CEA

Table 6 Systolic maximum velocity at some internal cross sections in cm/s measured with ECD and computed with numerical simulations. Level of the cross sections: Patient 1 before CEA: at the bifurcation; Patient 1 after CEA: at the begin of the ICA; Patient 2 before CEA: at a distance of 0.5cm from the begin of the ICA; Patient 2 after CEA: at a distance of 1.0cm from the begin of the ICA; Patient 3 before CEA: at the bifurcation; Patient 3 after CEA: at the begin of the ICA.

Figure 1

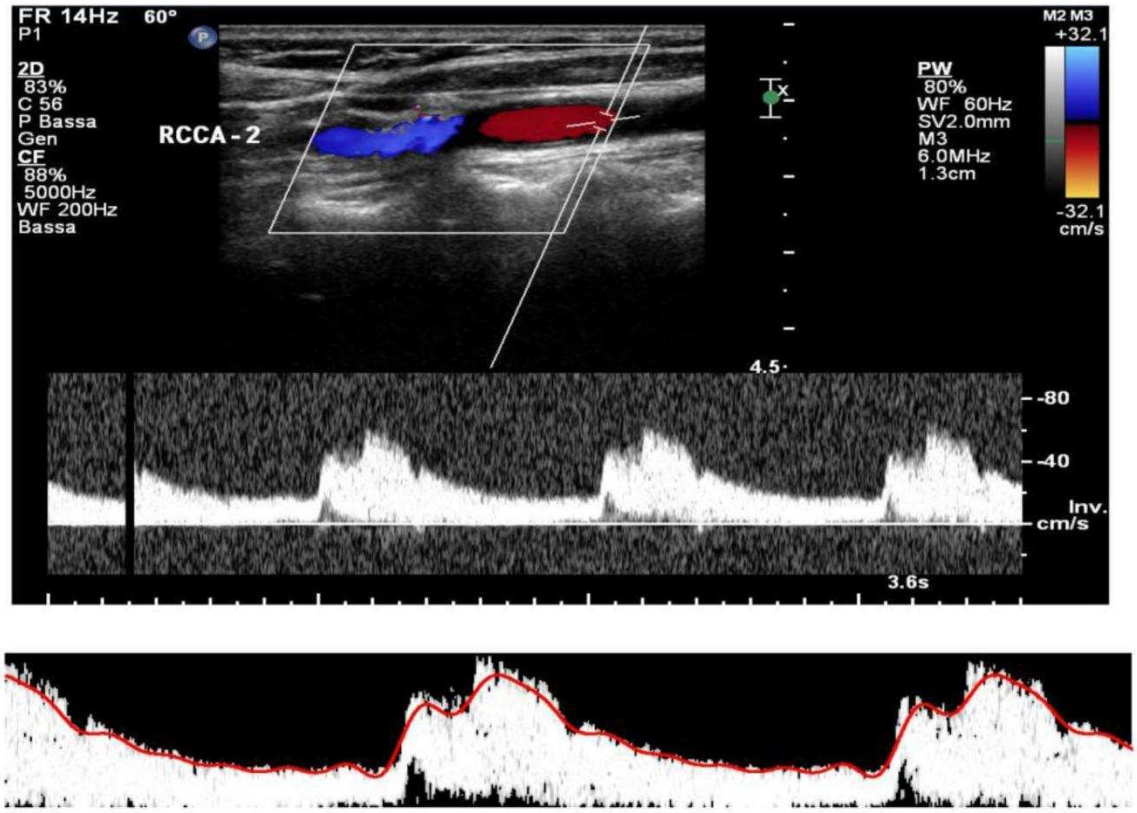
FR 14Hz
60°
P1
2D
83%
C 56
P Bassa
Gen
CF
88%
5000Hz
WF 200Hz
Bassa
RCCA - 2
PW
80%
WF 60Hz
SV2.0mm
M3
6.0MHz
1.3cm
M2 M3
+32.1
-32.1
cm/s
4.5
-80
-40
Inv.
cm/s
3.6s

Figure 2

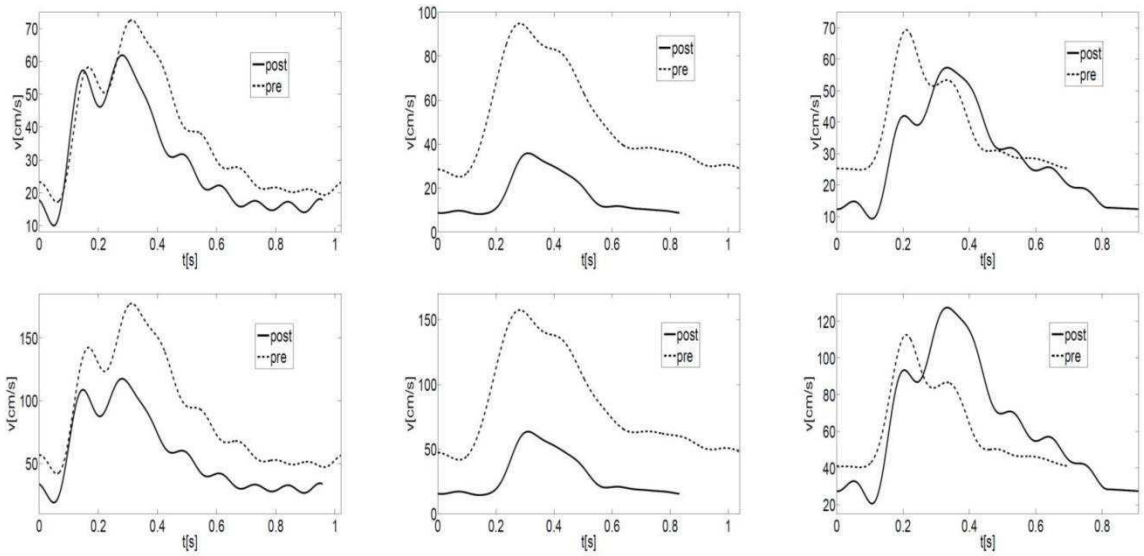

Figure 3

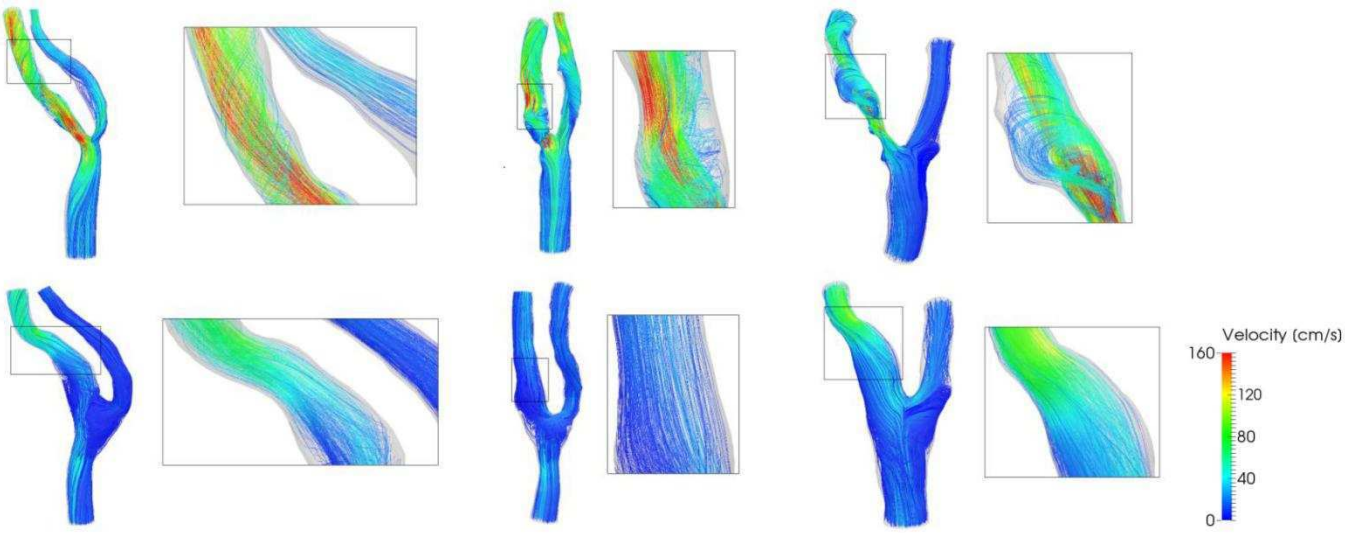

Figure 4

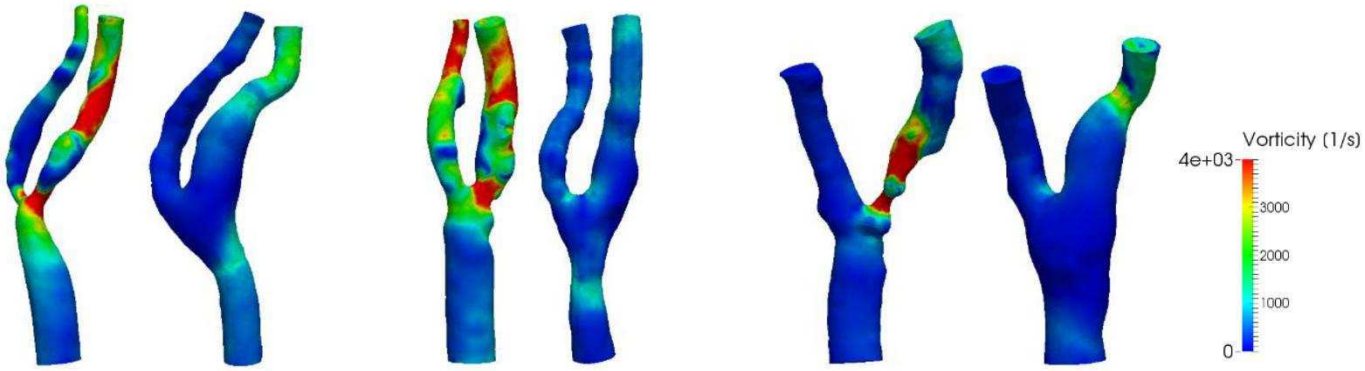

Figure 5

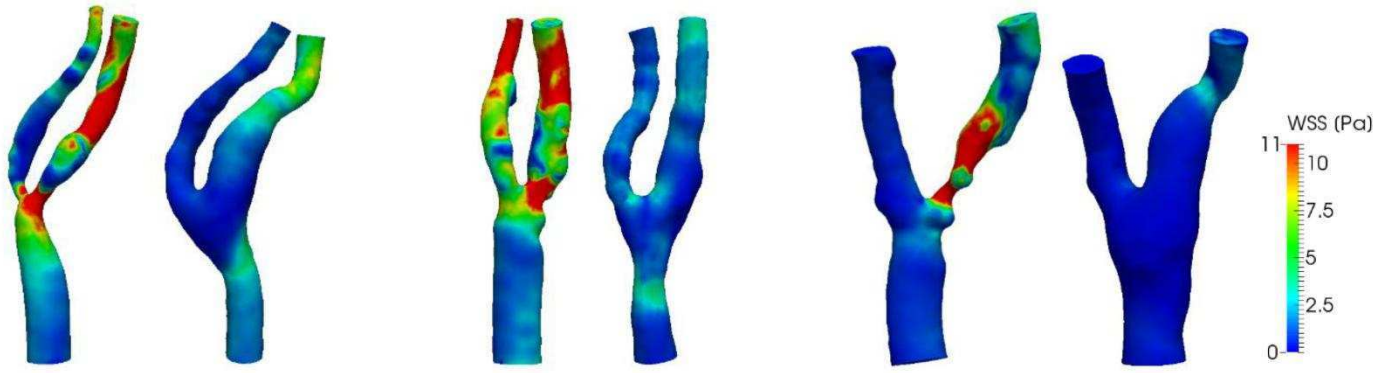

Table 1

	Age (years)	% of stenosis
Patient 1	65	75
Patient 2	81	80
Patient 3	81	90

Table 2

	Peak systolic velocity before CEA (cm/s)	Peak systolic velocity after CEA (cm/s)
Patient 1	333	117
Patient 2	209	63
Patient 3	288	127

Table 3

	Maximum vorticity before CEA (1/s)	Maximum vorticity after CEA (1/s)
Patient 1	6857	2902
Patient 2	7890	1448
Patient 3	8076	3279

Table 4

	Maximum WSS before CEA (Pa)	Maximum WSS after CEA (Pa)
Patient 1	36.2	4.8
Patient 2	27.4	4.6
Patient 3	36.7	5.8

Table 5

	Pressure drop before CEA (mmHg)	**Pressure drop after CEA (mmHg)**
Patient 1	27.6	3.0
Patient 2	11.6	1.3
Patient 3	21.1	3.5

Table 6

	Measured velocity (ECD)	Computed velocity
Patient 1 - before CEA	317.3	333.0
Patient 1 - after CEA	59.1	64.7
Patient 2 - before CEA	207.0	225.7
Patient 2 - after CEA	47.5	53.1
Patient 3 - before CEA	50.3	47.9
Patient 3 - after CEA	45.7	43.6